in vivo *33*: 2103-2111 (2019)
doi:10.21873/invivo.11710

A Population-based Statistical Model for Investigating Heterogeneous Intraprostatic Sensitivity to Radiation Toxicity After ^{125}I Seed Implantation

KAZUMA KOBAYASHI[1,2,3], NAOYA MURAKAMI[4], KANA TAKAHASHI[4], KOJI INABA[4], HIROSHI IGAKI[4], RYUJI HAMAMOTO[1,2,3] and JUN ITAMI[4]

[1]*Division of Molecular Modification and Cancer Biology, National Cancer Center Research Institute, Tokyo, Japan;*
[2]*Cancer Translational Research Team, RIKEN Center for Advanced Intelligence Project, Tokyo, Japan;*
[3]*Department of NCC Cancer Science, Graduate School of Medical and Dental Sciences, Tokyo Medical and Dental University, Tokyo, Japan;*
[4]*Department of Radiation Oncology, National Cancer Center Hospital, Tokyo, Japan*

Abstract. *Aim: To develop a population-based statistical model in order to find a spatial pattern of dose distribution which is related to lower urinary tract symptoms (LUTS) after iodine-125 (^{125}I) seed implantation for prostate cancer. Patients and Methods: A total of 75 patients underwent ^{125}I seed implantation for prostate cancer. Principal component analysis was applied to the standardized dose array and for each patient dose distribution was uniquely characterized by a combination of weighted eigenvectors. The correlation between eigenvectors and the severity of LUTS was investigated with linear regression analysis. Results: Eight eigenvectors were identified as being significantly associated with the severity of LUTS ($p<0.05$). Multivariate regression model identified that intraprostatic parameters, which were positively associated with the severity of LUTS, were distributed around a portion of the urethral base and a peripheral region of the prostate. Conclusion: We established a population-based statistical model that may indicate a significant dose pattern associated with the severity of radiation toxicity.*

Iodine-125 (^{125}I) seed implantation is a common treatment modality for localized prostate cancer. Whether brachytherapy is used as definitive monotherapy or as a boost combined with external beam radiotherapy (EBRT), it results in excellent tumor control rate (1-3) and is generally well tolerated (4, 5). Nevertheless, most patients develop either irritative or obstructive lower urinary tract symptoms (LUTS) to some degree. Although these symptoms eventually disappear from 12 to 18 months after the implantation (6-9), prolonged symptom and late symptom flare have also been reported (10-12). The risk of urinary toxicity is related to various factors, such as trauma caused by the procedure, prostate volume, pre-treatment International Prostate Symptom Score (IPSS) score or use of neoadjuvant hormonal therapy (13-16).

It is essential to optimize the dose distribution of brachytherapy in order to avoid adverse effects, however, the anatomical structures most critical in contributing to the development of LUTS remain to be elucidated. Recent evidence has suggested that the dose to specific subvolumes within the prostate might be more important than the dose to the whole prostate gland. Although the lower urinary tract segment (17, 18) and the urethral base/bladder neck (19-22) have been considered significant regions for urinary toxicity, there are some inconsistencies among studies (23). This is partly because current approaches to exploring the dose effect to organs at risk depends on the dose–volume histogram (DVH), which generally reduces the 3D dose distribution of the 2D histogram. Thus, if radiation toxicity is related not only to volumetric aspects of the dose, but also to the pattern of dose distribution, it is difficult for a DVH-based approach to detect it.

Finding a spatial pattern which predicts toxicity following radiotherapy is challenging because of different morphologies between patients (24). One remarkable application of image-processing for aligning radiation dose distributions was

Correspondence to: Kazuma Kobayashi, MD, Division of Molecular Modification and Cancer Biology, National Cancer Center Research Institute, 5-1-1, Tsukiji, Chuo-ku, Tokyo 104-0045, Japan. Tel: +81 335422511, Fax: +81 335453567, e-mail: kazumkob@ncc.go.jp

Key Words: Prostate cancer, brachytherapy, heterogeneous intra-organ radiosensitivity, non-rigid registration, principal component analysis.

proposed by Liang *et al*. (25). Using an optical flow-based deformable registration method, they remapped each patient's dose distribution to a template structure and revealed a subregion of the bone marrow critical for acute hematological and radiation toxicity. More recently, Jiang *et al*. combined deformable registration for the structural information of salivary glands and machine learning techniques to identify the spatial pattern of the dose associated with the severity of post-radiation xerostomia (26). These methods have great potential in identifying vulnerable subregions with a spatial consideration, therefore, we tried to extend the framework for cases with prostate cancer treated by ^{125}I seed implantation.

In order to identify a spatial pattern associated with the development of LUTS after brachytherapy, we developed an in-house method with contour-based non-rigid deformable registration (27, 28). Firstly, we created a population-based average shape of the prostate as a reference frame. Each patient's dose grid was mapped to the coordinate space of the reference frame, resulting in a standardized dose array with 25,950 variables. Because each row in the dose array corresponded to a specific voxel in the common reference frame, the standardized array allowed us to compare each patient's spatial dose distribution. Further, principal component analysis (PCA) was applied to the data set. PCA is a technique for reducing the dimensionality of a data set. In the present study, PCA generated 75 eigenvectors with descending order of explained variance ratio for the variability of the severity of LUTS. Because each individual dose array was summarized by a linear combination of weighted eigenvectors, it was possible to evaluate their correlation with the severity of LUTS by regression analysis. Finally, 3D parameterization of the sum of eigenvectors weighted by the regression coefficients was analyzed in order to identify a subvolume critical for the development of LUTS after ^{125}I seed implantation.

Patients and Methods

Patient and treatment. From May 2009 to December 2013, 80 consecutive patients underwent ^{125}I seed implantation with a prescribed dose of 160 Gy at our Institution. Our treatment protocol and technique for localized prostate cancer is described in detail elsewhere (29). Of the 80 patients, five patients were excluded because of the insufficient data of IPSS scores before or after the brachytherapy. Clinical characteristics of the 75 patients were summarized in Table I. The median age was 71 years (range=52-86 years). The follow-up time was a minimum of 12 months. According to the National Comprehensive Cancer Network risk classification (30), the majority of patients (n=51, 68.0%) were in the intermediate-risk group. Seventy-four patients (98.6%) received an α-blocker for as long as urinary symptoms persisted. The dose distribution was calculated based on computed tomographic scan 1 month after the brachytherapy.

For scoring of LUTS, the IPSS questionnaire was used. Patients' IPSS scores were obtained before brachytherapy and repeated at each follow-up visit after the treatment. Patients were evaluated every 3 months for the first year. The maximum increase of IPSS from the pretreatment score during the first year after the treatment was calculated for each patient. IPSS scores and toxicity data were collected retrospectively from the database.

Table I. *Patient characteristics (n=75).*

Characteristic	Value
Age, years	
Median (range)	71 (52-86)
T-Stage, n (%)*	
T1c	48 (64.0%)
T2a	19 (25.3%)
T2b	2 (2.6%)
T2c	3 (4.0%)
T3a	1 (1.3%)
T3b	1 (1.3%)
Unknown	1 (1.3%)
N-Stage, n (%)*	
N0	74 (98.6%)
N1	1 (1.3%)
M-Stage, n (%)*	
M0	75 (100.0%)
PSA	
Median (range)	6.25 (1.3-93)
≤10 ng/ml, n (%)	15 (20.0%)
>10 ng/ml, n (%)	60 (80.0%)
Gleason score	
Median (range)	7 (5-9)
≤7, n (%)	53 (70.6%)
>7, n (%)	22 (29.3%)
NCCN risk classification, n (%)	
High	6 (8.0%)
Intermediate	51 (68.0%)
Low	18 (24.0%)
Hormone therapy, n (%)	
Neoadjuvant	15 (20.0%)
Adjuvant	3 (4.0%)

PSA: Prostate-specific antigen; NCCN: National Comprehensive Cancer Network: Prostate Cancer (Version 4.2018) (30).

Image processing framework. The analysis was performed using in-house developed software which was written in Python using VTK/ITK library and a module of robust point set registration based on Gaussian mixture model (GMM) whose efficacy and validity were proven by Jian and Vemuri (31).

Firstly, we created a reference frame for the dose analysis. Based on contour data from the Digital Imaging and Communications in Medicine (DICOM) exported by Variseed (Varian Medical Systems, Palo Alto, CA, USA), the generated surface mesh consisted of both prostate and an intraprostatic urethra for each patient. Of 75 prostates, we selected one prostate whose volume was the closest to the average volume of the 75 prostates as a template for subsequent registration. After adjusting each coordinate origin to each center of mass of the prostate, non-rigid registration based on GMM was performed to find a transformation function between the template mesh and the remaining 74 meshes. When applying the

module published by Jian and Vemuri (31), control points were created so as to be distributed on the surface mesh at a regular interval of 2 mm. The number of iterative optimizations was set to 2. The scale factor was 0.4 and 0.16 in the first and second annealing step, respectively. The surface distance error (32), which is defined by a mean distance between the transformed surface points and the target surface, was less than 1 mm in all the cases. Consequently, the transformation function computed vectors connecting points on the template mesh to the surface of the remaining 74 meshes. We referred to these vectors as residue displacement vectors (33). By adding mean displacement vectors at each control point of the template structure, we created a population-based average shape of the prostate with the intraprostatic urethra. Hereafter, we considered the average shape of the prostate with intraprostatic urethra the reference frame.

Next, we tried to compare the spatial dose distribution among patients by using the reference frame. Our contour-based registration process consisted of two steps: (i) Surface registration based on GMM, and (ii) inner point set transformation by using thin-plate spline function. Firstly, non-rigid deformable registration based on GMM of the reference frame to each patient's prostate with intraprostatic urethra was performed. The parameters of the registration module were the same as described above. Subsequently, inner points were set as 1.0×1.0×1.0 mm^3, resulting in 25,950 voxels inside the reference frame. Internal voxels were remapped to each patient's original coordinate based on a vector field computed by a thin-plate spline function. A parameter to control the rigidity of the transformation was tuned and visually inspected. Consequently, radiation doses of the patients were standardized to the voxels in the reference frame (Figure 1). Because each row in the dose array corresponded to a specific voxel in the reference frame, the standardized array allowed us to compare each patient's spatial dose distribution.

Detecting heterogeneous intraprostatic radiosensitivity. Our approach for detecting heterogeneous intraprostatic radiosensitivity was inspired by previous studies (25, 34).

PCA is a statistical technique useful for reducing the dimension of data with a large number of variables. Firstly, each patient's dose distribution remapped on the reference frame was sampled from left to right, from anterior to posterior, and from inferior to superior. Sampled doses were concatenated to form a row vector di with 25,950 variables for the ith patient. Next, stacking 75 row vectors of all patients (d_1,…,d_{75}) resulted in an N×M matrix, here 75×25,950 matrix D as a high-dimensional data set. PCA was applied to the covariance matrix of D using singular value decomposition and generated 75 eigenvectors (e_1,…e_{75}) with 25,950 variables arranged in descending order of the explained variance ratio of the data set. The dose array of the i*th* patient was then uniquely represented by a linear combination of eigenvectors and weighted parameters θ_i, which was termed the principal component score:

$$d_i = \sum_{k=1}^{N} \theta_{ik} e_k$$

To find a spatial pattern associated with the development of LUTS, univariate linear regression analysis was applied to an objective variable y, as the maximum increase of IPSS after the treatment, for each principal component score (θ_1,…θ_{75}) as a predictor variable. Statistical significance was set at a two-sided p-value of less than 0.10. Significant eigenvectors obtained by the univariate model were subsequently incorporated into multivariate linear regression analysis. The multivariate analysis identified a few significant eigenvectors $(e_k)_{k\in I}$ associated with the development of LUTS, with statistical significance at $p<0.05$. Thus, we formulated a model to predict the clinical outcome using the subset of significant eigenvectors and regression coefficients β_k as follows:

$$y_i = \sum_{k\in I} \beta_k \theta_{ik}$$

Because the i*th* principal component score can be obtained by the inner product between ei and di ($\theta_{ik}=e_k\, d_i$), the above formula can be transformed:

$$y_i = \sum_{k\in I} \beta_k e_k d_i$$

By defining the parameter function v as the sum of the significant eigenvectors weighted by the regression coefficients ($v=\sum_{k\in I}\beta_k e_k$), a new patient's maximum increase of IPSS can be predicted using the patient's dose vector d as follows

$$y=vd$$

Importantly, the proposed model is based on the assumption that urinary toxicity is given by the sum of all the individual contributions of intraprostatic subvolumes. The estimated parameter function v provides information about the volume effects of each voxel in the development of LUTS. The spatial representation of the parameters of v indicates heterogeneous intraprostatic sensitivity to radiation.

Statistical analysis. For the linear regression analysis, JMP version 10.0 (SAS Institute, Cary, NC, USA) was used. PCA was performed by the in-house developed software written in Python.

Results

PCA of the dose array. The result of PCA of the standardized dose array generated a set of 75 eigenvectors. The first three eigenvectors of the covariance matrix are shown in Figure 2, indicating the three largest modes of variation of the dose distribution and intensity. The patterns showed that the major directions of variance were the whole prostate gland (eigenvector 1), followed by the superior/inferior (eigenvector 2) and central/peripheral (eigenvector 3) regions of the prostate.

Regression analysis of eigenvectors for IPSS increase. Eight eigenvectors (27th, 28th, 38th, 41th, 47th, 70th, 71th, and 74th) were identified that were significantly associated with the maximum increase in IPSS using the linear regression model (Table II). The ratios of the explained variance of the original data demonstrated by these eight eigenvectors were 1.07×10^{-2}, 1.03×10^{-2}, 0.78×10^{-2}, 0.71×10^{-2}, 0.63×10^{-2},

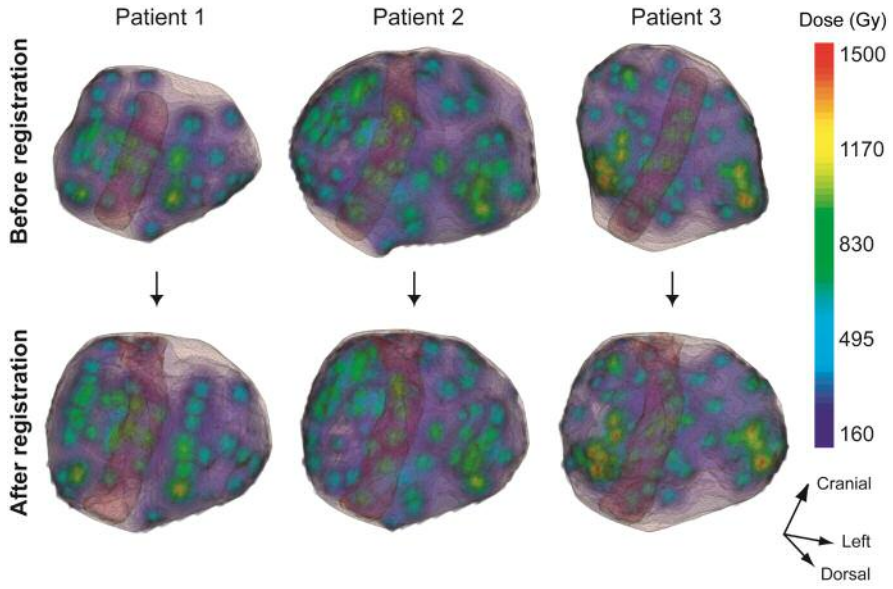

Figure 1. *Example prostate (outer mesh) with the intraprostatic urethra (inner mesh) showing the remapped dose distribution after registration. Each patient's intraprostatic dose distribution was transformed by the contour-based non-rigid registration to the reference frame, which was the average shape of the 75 patients' prostate glands.*

0.3×10^{-2}, 0.33×10^{-2} and 0.27×10^{-2}, respectively. The regression model had an R^2 value of 41.6%, indicating that it accounted for 41.6% of the variation in the maximum increase of IPSS score. The adjusted R^2 value of the model was 34.5%.

Heterogeneous intraprostatic radiosensitivity. The summation of significant eigenvectors (27th, 28th, 38th, 41th, 47th, 70th, 71th, and 74th) weighted by each regression coefficient (β_{27}, β_{28}, β_{38}, β_{41}, β_{47}, β_{70}, β_{71} and β_{74}) represented the parameter function v. Because a new patient's maximum increase of IPSS after the treatment can be estimated by $y=vd$, the 3D representation of v indicates heterogeneous intraprostatic sensitivity to radiation (Figure 3A). Furthermore, in order to compare with the parameter function v, we divided the patients into two groups aaccording to maximum increase in IPSS: those with a maximum increase of 20 (75th percentile) or less (n=58), and those with a maximum increase of more than 20 (n=17). By directly subtracting the average dose of the latter group from that of the former, the difference in radiation dose between the two groups was represented in the reference frame (Figure 3B).

In order to help understand the spatial patterns of parameter distribution in the reference frame, a projected diagram according to the distance from the urethra was created (Figure 4). In the diagram, each voxel was stratified by its distance from the urethra at a regular interval of 1 mm in each axial plane, and an average value of each stratified group was represented as a function of both the distance from the urethra and the distance from the prostate apex. Like the axial plane, it was also sampled at a regular interval of 1 mm.

The projected diagram of the parameter function v (Figure 5A) showed two hotspots in the prostate: one was located surrounding the urethral base (Figure 5A, arrow), and the other was at the peripheral site of the prostate (Figure 5A, arrowhead). These two hotspots were also correspondingly observed in a projected diagram of the dose difference model (Figure 5B).

Discussion

To the best of our knowledge, this is the first study to apply contour-based non-rigid registration and PCA-based regression with the aim of identifying specific intraprostatic subvolumes sensitive to the development of LUTS after prostate brachytherapy. The proposed method identified two possible responsible regions; one surrounding the urethral base (Figure 5A, arrow), and the other is at the peripheral site of the prostate (Figure 5A, arrowhead). Since the peripheral site is a relatively long distance from the urethra, the interpretation for coefficients in the region is not clear and there remains a possibility that these may be noise from particular bias in the dataset from the viewpoint of radiobiology. However, the result highlighted an apparent

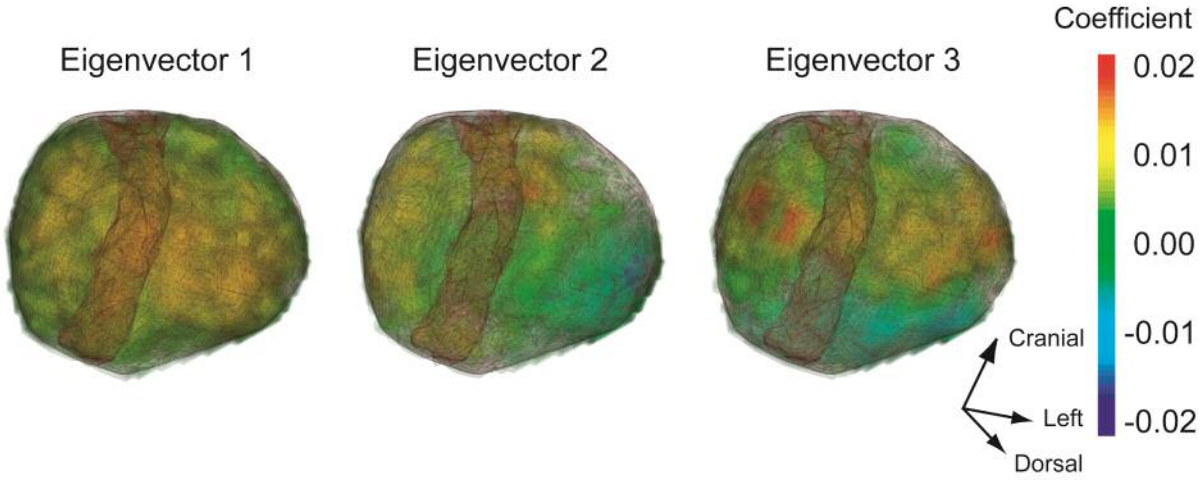

Figure 2. *The first three eigenvectors of the covariance matrix, showing major modes of variation in the data set. The major tendency of variance was the whole prostate gland (eigenvector 1), and the superior/inferior (eigenvector 2) and central/peripheral (eigenvector 3) regions.*

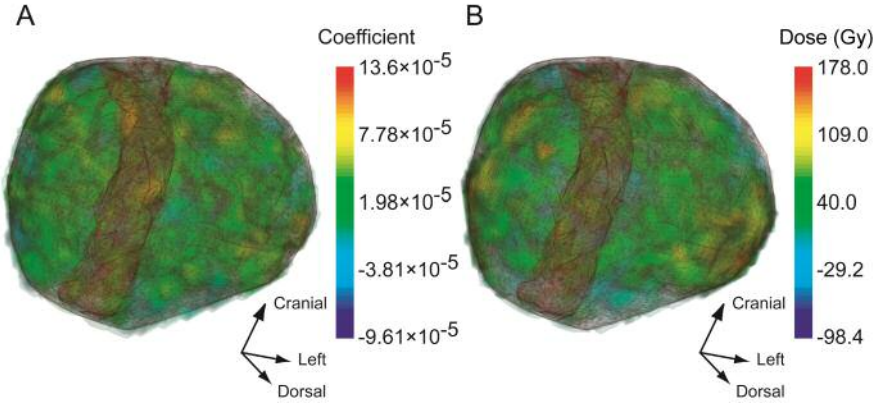

Figure 3. *Results of principal component analysis regression analysis. A: Linear combination of significant eigenvectors weighted by significant regression coefficients represented a spatial parameter distribution associated with the development of lower urinary tract symptoms. B: Average dose difference between patients with and without International Prostate Symptom Score increase >20.*

Table II. *Significant results of principal component analysis multivariate regression.*

Principal component	Explained variance ratio	– β Value (95% CI)	*p*-Value
Intercept		14.44 (12.99-15.90)	<0.0001
27th	1.07×10^{-2}	8.12×10^{-4} (1.01×10^{-4}-15.24×10^{-4})	0.025
28th	1.03×10^{-2}	-9.66×10^{-4} (-16.90×10^{-4}- -2.42×10^{-4})	0.009
38th	0.78×10^{-2}	10.19×10^{-4} (1.87×10^{-4}-18.51×10^{-4})	0.017
41th	0.71×10^{-2}	-10.83×10^{-4} (-19.53×10^{-4}- -2.13×10^{-4})	0.015
47th	0.63×10^{-2}	-10.32×10^{-4} (-19.60×10^{-4}--1.04×10^{-4})	0.029
70th	0.34×10^{-2}	-13.49×10^{-4} (-25.99×10^{-4}- -0.99×10^{-4})	0.034
71th	0.33×10^{-2}	13.35×10^{-4} (0.59×10^{-4}-26.12×10^{-4})	0.040
74th	0.27×10^{-2}	-20.7×10^{-4} (-34.72×10^{-4}- -6.69×10^{-4})	0.004

CI: Confidence interval.

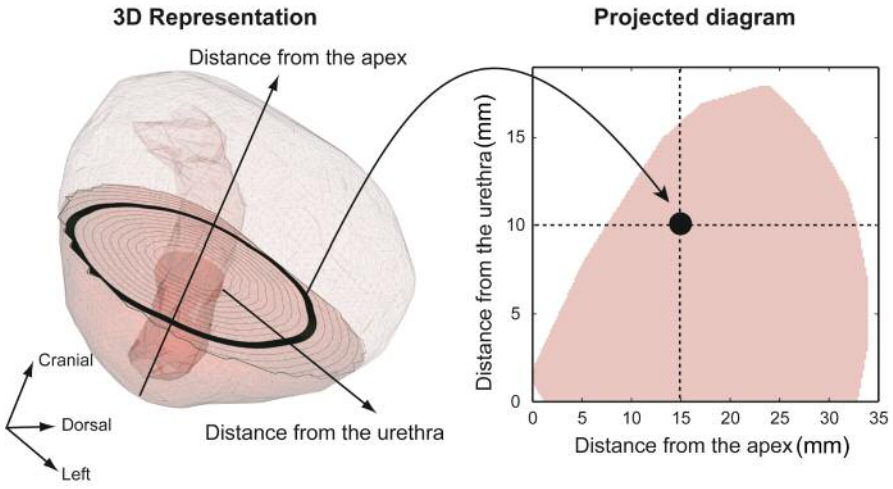

Figure 4. *Schematic representation of the projected diagram converted from the 3D representation of the reference frame. Each voxel was stratified by its distance from the urethra at an interval of 1 mm on each axial plane, and an average value of each stratified group is represented as a function of both distance from the urethra and distance from the prostate apex in the diagram.*

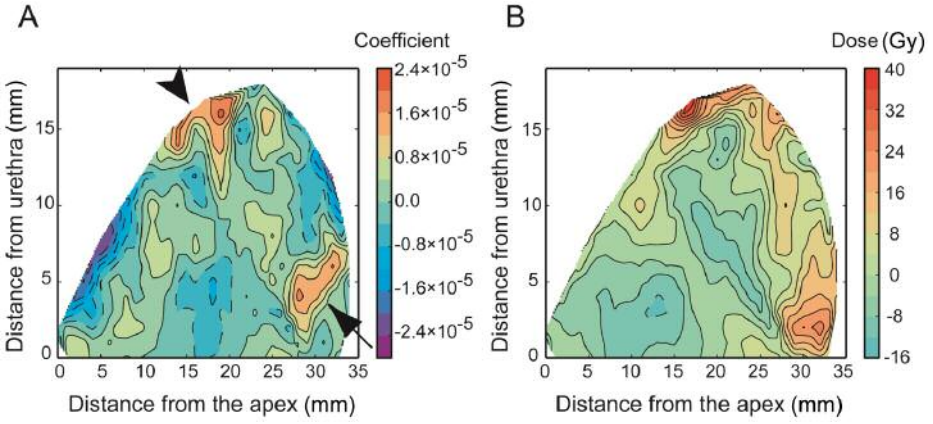

Figure 5. *Projected diagram of the data of Figure 3. A: The spatial parameter distribution showed that the prostate base (arrow) and the peripheral portion of the mid-prostate (arrowhead) were positively correlated with the development of lower urinary tract symptoms. B: The dose-difference model demonstrated these corresponding hotspots.*

propensity alongside the urethra, as higher coefficients were grouped at the outer peripheral side of the base rather than the apex (Figure 5A). This is consistent with the dose difference between the two groups with and without severe LUTS characterized by a maximum increase of IPSS>20 (Figure 5B). Consequently, we consider dose accumulation close to the urethral base may be associated with a higher likelihood of the development of LUTS.

LUTS is a frequent complication after ^{125}I seed implantation, however, the results of previous studies focused on the critical structure for its development are not consistent. Several prior studies suggested a correlation between the urethral dose and urinary toxicity (18, 35-37), whereas others have not supported this (22, 23, 38). This is partly because the development of LUTS might be a complicated phenomenon, which may be influenced by other factors such as trauma and number of needles used for seed implantation (13-15, 17, 39), pretreatment IPSS (16), pretreatment urinary flow (8) and neoadjuvant hormone therapy (40). Still, it is theoretically possible that the dose to different segments of the prostate or urinary tract might contribute to the substantial risk of LUTS. Williams *et al.*

reported a positive correlation between the number of seeds above the prostate base and an increase of IPSS (8) and discussed a possible effect on the bladder neck from seeds. Pinkawa *et al*. suggested the dose to the seminal vesicle to be closely related to the dose to the bladder neck and urethral sphincter muscle, contributing to late urinary dysfunction (41). Notably, Thomas *et al*. found that a higher urethral dose to the prostate base was associated with higher maximum IPSS scores, by eliminating all known factors predicting for urinary morbidity (20). In addition, Pinkawa *et al*. demonstrated that seeds implanted in close vicinity of the urethra had a significant impact on urinary morbidity irrespective of the urethral DVH (42).

The contribution of our research is to add a new observation to the line of evidence by using a modern image-processing technique which does not need any manual segmentation to divide the hypothetical segments for the prostate and the urethra. Because the PCA-based approach is able to extract the specific dose pattern responsible for the development of LUTS in the dataset (Table II), we can explain what kind of dose pattern has a particular weight for the prediction by the model. This is quite important because it enables us to quantitatively evaluate the intra-organ spatial dependence associated with the occurrence or the severity of radiation toxicity, leading to identification of the most critical subvolume within the organ in an explicit manner. The suggested region surrounding the urethral base (Figure 5A, arrow) was consistent with the results of several previous studies (8, 18, 20, 41), implying that the proposed method can work at least as a screening technique. Moreover, because there are many organs which do not have distinct boundaries on imaging, our contour-based approach can easily be applied to investigations of the spatial dose pattern for various volumes of interest delineated in treatment planning systems. Owing to the higher accuracy and feasibility of contour-based deformable registration in comparison with an intensity-based algorithm, the contour-based approach can be employed in handling organs with large deformation, such as organs in the pelvic region (28, 32).

There are several limitations to this study. The present study included a relatively small number of patients and was retrospectively designed so that some inherent biases might exist. The contribution of the intraprostatic irradiation profile to the development of LUTS was moderate, as shown by the adjusted R2 value of 34.5% in the data set. The proposed method did not exclude any confounding factors for the relationship between the intraprostatic dose distribution and LUTS. Thus, we considered that positive coefficients in the peripheral site of the prostate (Figure 5A, arrowhead) might reflect some bias or confounding effects, which may have resulted from the procedure or other clinical factors. Further investigation with an extended approach, which can incorporate multivariate analysis, in a large cohort is necessary.

Conclusion

The region of the prostate surrounding the urethral base might be associated with a maximum increase of IPSS after ^{125}I seed implantation. Our heuristic framework without a priori consideration of segmentation might have a wide clinical application intra-organ heterogeneous sensitivity to radiation.

Conflicts of Interest

Authors have no conflict of interest to declare.

Authors' Contributions

All Authors made substantial contributions to conception and design, acquisition of data, and analysis and interpretation of data: K.K., N.M., K.T. and K.I. collected cases. K.K. completed all data. K.K. and N.M. designed the study and analyzed data. K.K., N.M., and J.I. co-wrote the article. R.H. and J.I. critically revised the article.

Acknowledgements

This work was financially supported by Grants in-Aid for Young Scientists (B) from the Ministry of Education, Culture, Sports, Science, and Technology of Japan (Grant number 17K16497).

References

1 Hinnen KA, Battermann JJ, van Roermund JGH, Moerland MA, Jürgenliemk-Schulz IM, Frank SJ and van Vulpen M: Long-term biochemical and survival outcome of 921 patients treated with I-125 permanent prostate brachytherapy. Int J Radiat Oncol *76*: 1433-1438, 2010. PMID: 19540075. DOI: 10.1016/j.ijrobp.2009.03.049

2 Zelefsky MJ, Kuban DA, Levy LB, Potters L, Beyer DC, Blasko JC, Moran BJ, Ciezki JP, Zietman AL, Pisansky TM, Elshaikh M and Horwitz EM: Multi-institutional analysis of long-term outcome for stages T1-T2 prostate cancer treated with permanent seed implantation. Int J Radiat Oncol *67*: 327-333, 2007. PMID: 17084558. DOI: 10.1016/j.ijrobp.2006.08.056

3 Potters L, Morgenstern C, Calugaru E, Fearn P, Jassal A, Presser J and Mullen E: 12-Year outcomes following permanent prostate brachytherapy in patients with clinically localized prostate cancer. J Urol *173*: 1562-1566, 2005. PMID: 15821486. DOI: 10.1097/01.ju.0000154633.73092.8e

4 Stone NN and Stock RG: Complications following permanent prostate brachytherapy. Eur Urol *41*: 427-433, 2002. PMID: 12074815. DOI: 10.1016/S0302-2838(02)00019-2

5 Anderson J, Swanson D, Levy L, Kuban D, Lee A, Kudchadker R, Phan J, Bruno T and Frank S: Urinary side effects and complications after permanent prostate brachytherapy: The MD Anderson Cancer Center experience. Urology *74*: 601-605, 2009. PMID: 19589580. DOI: 10.1016/j.urology.2009.04.060

6 Bottomley D, Ash D, Al-Qaisieh B, Carey B, Joseph J, St Clair S and Gould K: Side effects of permanent ^{125}I prostate seed implants in 667 patients treated in Leeds. Radiother Oncol *82*:

46-49, 2007. PMID: 17161481. DOI: 10.1016/j.radonc.2006.11.006

7 Van Gellekom MPR, Moerland M, Van Vulpen M, Wijrdeman HK and Battermann JJ: Quality of life of patients after permanent prostate brachytherapy in relation to dosimetry. Int J Radiat Oncol Biol Phys *63*: 772-780, 2005. PMID: 15964707. DOI: 10.1016/j.ijrobp.2005.03.046

8 Williams SG, Millar JL, Duchesne GM, Dally MJ, Royce PL and Snow RM: Factors predicting for urinary morbidity following 125iodine transperineal prostate brachytherapy. Radiother Oncol *73*: 33-38, 2004. PMID: 15465143. DOI: 10.1016/j.radonc.2004.07.026

9 Tanaka N, Yorozu A, Kikuchi T, Higashide S, Kojima S, Ohashi T, Katayama N, Nakamura K, Saito S, Dokiya T, Fukushima M and J-POPS Study Group: Genitourinary toxicity after permanent iodine-125 seed implantation: The nationwide Japanese prostate cancer outcome study of permanent iodine-125 seed implantation (J-POPS). Brachytherapy *18*: 484-492, 2019. PMID: 31072729. DOI: 10.1016/j.brachy.2019.03.007

10 Caffo O, Fellin G, Bolner A, Coccarelli F, Divan C, Frisinghelli M, Mussari S, Ziglio F, Malossini G, Tomio L and Galligioni E: Prospective evaluation of quality of life after interstitial brachytherapy for localized prostate cancer. Int J Radiat Oncol Biol Phys *66*: 31-37, 2006. PMID: 16765529. DOI: 10.1016/j.ijrobp.2006.04.009

11 Cesaretti JA, Stone NN and Stock RG: Urinary symptom flare following I-125 prostate brachytherapy. Int J Radiat Oncol *56*: 1085-1092, 2003. PMID: 12829146. DOI: 10.1016/S0360-3016(03)00210-4

12 Frank SJ, Pugh TJ, Blanchard P, Mahmood U, Graber WJ, Kudchadker RJ, Davis JW, Kim J, Choi H, Troncoso P, Kuban DA, Choi S, McGuire S, Hoffman KE, Chen H-C, Wang X and Swanson DA: Prospective phase 2 trial of permanent seed implantation prostate brachytherapy for intermediate-risk localized prostate cancer: Efficacy, toxicity, and quality of life outcomes. Int J Radiat Oncol *100*: 374-382, 2018. PMID: 29229325. DOI: 10.1016/j.ijrobp.2017.09.050

13 Eapen L, Kayser C, Deshaies Y, Perry G, E C, Morash C, Cygler JE, Wilkins D and Dahrouge S: Correlating the degree of needle trauma during prostate brachytherapy and the development of acute urinary toxicity. Int J Radiat Oncol Biol Phys *59*: 1392-1394, 2004. PMID: 15275724. DOI: 10.1016/j.ijrobp.2004.01.041

14 Keyes M, Schellenberg D, Moravan V, McKenzie M, Agranovich A, Pickles T, Wu J, Liu M, Bucci J and Morris WJ: Decline in urinary retention incidence in 805 patients after prostate brachytherapy: the effect of learning curve? Int J Radiat Oncol Biol Phys *64*: 825-834, 2006. PMID: 16458775. DOI: 10.1016/j.ijrobp.2005.04.056

15 Wust P, von Borczyskowski DW, Henkel T, Rosner C, Graf R, Tilly W, Budach V, Felix R and Kahmann F: Clinical and physical determinants for toxicity of 125-I seed prostate brachytherapy. Radiother Oncol *73*: 39-48, 2004. PMID: 15465144. DOI: 10.1016/j.radonc.2004.08.003

16 Keyes M, Miller S, Moravan V, Pickles T, McKenzie M, Pai H, Liu M, Kwan W, Agranovich A, Spadinger I, Lapointe V, Halperin R and Morris WJ: Predictive factors for acute and late urinary toxicity after permanent prostate brachytherapy: long-term outcome in 712 consecutive patients. Int J Radiat Oncol Biol Phys *73*: 1023-1032, 2009. PMID: 19111402. DOI: 10.1016/j.ijrobp.2008.05.022

17 Roeloffzen EM a, Monninkhof EM, Battermann JJ, van Roermund JGH, Moerland M a and van Vulpen M: Acute urinary retention after I-125 prostate brachytherapy in relation to dose in different regions of the prostate. Int J Radiat Oncol Biol Phys *80*: 76-84, 2011. PMID: 20605364. DOI: 10.1016/j.ijrobp.2010.01.022

18 Singhal S, Jamaluddin MF, Lee E, Sloboda RS, Parliament M and Usmani N: Clinical factors and dosimetry associated with the development of prostate brachytherapy-related urethral strictures: A matched case-control study. Brachytherapy *16*: 797-805, 2017. PMID: 28578920. DOI: 10.1016/j.brachy.2017.04.242

19 Steggerda MJ, Witteveen T, van den Boom F and Moonen LMF: Is there a relation between the radiation dose to the different sub-segments of the lower urinary tract and urinary morbidity after brachytherapy of the prostate with I-125 seeds? Radiother Oncol *109*: 251-255, 2013. PMID: 24060176. DOI: 10.1016/j.radonc.2013.07.019

20 Thomas C, Keyes M, Liu M and Moravan V: Segmental urethral dosimetry and urinary toxicity in patients with no urinary symptoms before permanent prostate brachytherapy. Int J Radiat Oncol Biol Phys *72*: 447-455, 2008. PMID: 18395357. DOI: 10.1016/j.ijrobp.2007.12.052

21 Ghadjar P, Zelefsky MJ, Spratt DE, Munck af Rosenschöld P, Oh JH, Hunt M, Kollmeier M, Happersett L, Yorke E, Deasy JO and Jackson A: Impact of dose to the bladder trigone on long-term urinary function after high-dose intensity modulated radiation therapy for localized prostate cancer. Int J Radiat Oncol Biol Phys *88*: 339-344, 2014. PMID: 24411606. DOI: 10.1016/j.ijrobp.2013.10.042

22 Hathout L, Folkert MR, Kollmeier M a, Yamada Y, Cohen GN and Zelefsky MJ: Dose to the bladder neck is the most important predictor for acute and late toxicity after low-dose-rate prostate brachytherapy: implications for establishing new dose constraints for treatment planning. Int J Radiat Oncol Biol Phys 90: 312-319, 2014. PMID: 25304791. DOI: 10.1016/j.ijrobp.2014.06.031

23 Allen ZA, Merrick GS, Butler WM, Wallner KE, Kurko B, Anderson RL, Murray BC and Galbreath RW: Detailed urethral dosimetry in the evaluation of prostate brachytherapy-related urinary morbidity. Int J Radiat Oncol Biol Phys *62*: 981-987, 2005. PMID: 15989998. DOI: 10.1016/j.ijrobp.2004.12.068

24 Kobayashi K: Modern computational technologies for establishing precision brachytherapy: From non-rigid image registration to deep learning. *In*: Brachytherapy. Singapore, Springer Singapore, pp. 23-34, 2019.

25 Liang Y, Messer K, Rose BS, Lewis JH, Jiang SB, Yashar CM, Mundt AJ and Mell LK: Impact of bone marrow radiation dose on acute hematologic toxicity in cervical cancer: Principal component analysis on high dimensional data. Int J Radiat Oncol Biol Phys *78*: 912-919, 2010. PMID: 20472344. DOI: 10.1016/j.ijrobp.2009.11.062

26 Jiang W, Lakshminarayanan P, Hui X, Han P, Cheng Z, Bowers M, Shpitser I, Siddiqui S, Taylor RH, Quon H and McNutt T: Machine learning methods uncover radiomorphologic dose patterns in salivary glands that predict xerostomia in patients with head and neck cancer. Adv Radiat Oncol *4*: 401-412, 2019. PMID: 31011686. DOI: 10.1016/J.ADRO.2018.11.008

27 Bing Jian and Vemuri BC: Robust point set registration using Gaussian mixture models. IEEE Trans Pattern Anal Mach Intell

33: 1633-1645, 2011. PMID: 21173443. DOI: 10.1109/TPAMI.2010.223

28 Kobayashi K, Murakami N, Wakita A, Nakamura S, Okamoto H, Umezawa R, Takahashi K, Inaba K, Igaki H, Ito Y, Shigematsu N and Itami J: Dosimetric variations due to interfraction organ deformation in cervical cancer brachytherapy. Radiother Oncol *117*: 555-558, 2015. PMID: 26316394. DOI: 10.1016/j.radonc.2015.08.017

29 Murakami N, Itami J, Okuma K, Marino H, Nakagawa K, Ban T, Nakazato M, Kanai K, Naoi K and Fuse M: Urethral dose and increment of international prostate symptom score (IPSS) in transperineal permanent interstitial implant (TPI) of prostate cancer. Strahlentherapie Und Onkol *184*: 515-519, 2008. PMID: 19016040. DOI 10.1007/s00066-008-1833-3

30 National Comprehensive Cancer Network: Prostate Cancer (Version 4.2018). Available from: https://www.nccn.org/professionals/physician_gls/pdf/prostate.pdf. Accessed August 15, 2018.

31 Jian B and Vemuri BC: A Robust Algorithm for Point Set Registration Using Mixture of Gaussians. Proc IEEE Int Conf Comput Vis *2*: 1246-1251, 2005. PMID: 19169422. DOI: 10.1109/ICCV.2005.17

32 Vásquez Osorio EM, Hoogeman MS, Bondar L, Levendag PC and Heijmen BJM: A novel flexible framework with automatic feature correspondence optimization for nonrigid registration in radiotherapy. Med Phys *36*: 2848-2859, 2009. PMID: 19673184. DOI: 10.1118/1.3134242

33 van der Wielen GJ, Mutanga TF, Incrocci L, Kirkels WJ, Vasquez Osorio EM, Hoogeman MS, Heijmen BJM and de Boer HCJ: Deformation of prostate and seminal vesicles relative to intraprostatic fiducial markers. Int J Radiat Oncol *72*: 1604-1611.e3, 2008. PMID: 19028284. DOI: 10.1016/j.ijrobp.2008.07.023

34 Benadjaoud MA, Blanchard P, Schwartz B, Champoudry J, Bouaita R, Lefkopoulos D, Deutsch E, Diallo I, Cardot H and de Vathaire F: Functional data analysis in NTCP modeling: a new method to explore the radiation dose-volume effects. Int J Radiat Oncol Biol Phys *90*: 654-663, 2014. PMID: 25304951. DOI: 10.1016/j.ijrobp.2014.07.008

35 Wallner K, Roy J and Harrison L: Dosimetry guidelines to minimize urethral and rectal morbidity following transperineal I-125 prostate brachytherapy. Int J Radiat Oncol Biol Phys *32*: 465-471, 1995. PMID: 7751187. DOI: 10.1016/0360-3016(94)00599-G

36 Zelefsky MJ, Yamada Y, Marion C, Sim S, Cohen G, Ben-Porat L, Silvern D and Zaider M: Improved conformality and decreased toxicity with intraoperative computer-optimized transperineal ultrasound-guided prostate brachytherapy. Int J Radiat Oncol Biol Phys *55*: 956-963, 2003. PMID: 12605973. DOI: 10.1016/S0360-3016(02)04142-1

37 Crook JM, Potters L, Stock RG and Zelefsky MJ: Critical organ dosimetry in permanent seed prostate brachytherapy: defining the organs at risk. Brachytherapy *4*: 186-194, 2005. PMID: 16182218. DOI: 10.1016/j.brachy.2005.01.002

38 Neill M, Studer G, Le L, McLean M, Yeung I, Pond G and Crook JM: The nature and extent of urinary morbidity in relation to prostate brachytherapy urethral dosimetry. Brachytherapy *6*: 173-179, 2007. PMID: 17681239. DOI: 10.1016/j.brachy.2007.03.003

39 Salembier C, Lavagnini P, Nickers P, Mangili P, Rijnders A, Polo A, Venselaar J and Hoskin P: Tumour and target volumes in permanent prostate brachytherapy: A supplement to the ESTRO/EAU/EORTC recommendations on prostate brachytherapy. Radiother Oncol *83*: 3-10, 2007. PMID: 17321620. DOI: 10.1016/j.radonc.2007.01.014

40 Stone NN, Gerber NK, Blacksburg S, Stone J and Stock RG: Factors influencing urinary symptoms 10 years after permanent prostate seed implantation. J Urol *187*: 117-123, 2012. PMID: 22114818. DOI: 10.1016/j.juro.2011.09.045

41 Pinkawa M, Fischedick K, Piroth MD, Gagel B, Borchers H, Jakse G and Eble MJ: Health-related quality of life after permanent interstitial brachytherapy for prostate cancer. Strahlentherapie und Onkol *182*: 660-665, 2006. PMID: 17072524. DOI: 10.1007/s00066-006-1530-z

42 Pinkawa M, Holy R, Piroth MD, Klotz J, Pfister D, Heidenreich A and Eble MJ: Urinary morbidity after permanent prostate brachytherapy – impact of dose to the urethra *vs*. sources placed in close vicinity to the urethra. Radiother Oncol *103*: 247-251, 2012. PMID: 22300607. DOI: 10.1016/j.radonc.2011.12.011

Received August 2, 2019
Revised August 28, 2019
Accepted September 3, 2019